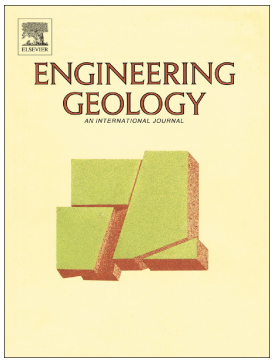


# Seismic monitoring system for landslide hazard assessment and risk management at the drainage plant of the Peschiera Springs (Central Italy)

Roberto Iannucci, Luca Lenti, Salvatore Martino

PII: S0013-7952(20)30280-5

DOI: https://doi.org/10.1016/j.enggeo.2020.105787

Reference: ENGEO 105787

To appear in: *Engineering Geology*

Received date: 14 February 2020

Revised date: 19 July 2020

Accepted date: 29 July 2020

Please cite this article as: R. Iannucci, L. Lenti and S. Martino, Seismic monitoring system for landslide hazard assessment and risk management at the drainage plant of the Peschiera Springs (Central Italy), *Engineering Geology* (2020), https://doi.org/10.1016/j.enggeo.2020.105787

# Seismic monitoring system for landslide hazard assessment and risk management at the drainage plant of the Peschiera Springs (Central Italy)

Roberto Iannucci[1*], Luca Lenti[2,3], Salvatore Martino[1]

[1] *Dipartimento di Scienze della Terra & Centro di Ricerca per i Rischi Geologici CERI, Sapienza Università di Roma, P.le A. Moro 5, 00185 Roma, Italy.*
[2] *Université Gustave Eiffel, IFSTTAR (GERS/SRO), 14-20 Boulevard Newton, Cité Descartes, Champs-sur-Marne, F-77447 Marne la Vallée Cedex 2, France.*
[3] *Equipe-Project MOUVGS, Centre d'Études et d'Expertise sur les Risques, l'Environnement, la Mobilité et l'Aménagement CEREMA, 500 Route des Lucioles, Sophia-Antipolis, F-06903, France.*
[*] *Corresponding Author E-mail: roberto.iannucci@uniroma1.it Telephone:+39 0649914835*

**Keywords**: Microseismic event analysis; Nanoseismic monitoring; Seismic network; Mass rock creep; Landslide hazard assessment; Landslide risk management

## Highlights

- Analysis of microseismic events recorded by two seismic systems in an unstable slope.
- Assessing of landslide hazard by microseismic event analysis.
- Implementation of an automatic procedure to analyse microseismic events.
- Integration of seismic systems to manage and drainage plant located within the slope.

## Abstract

The assessment of landslide hazards and design of strategies for managing the related risk have been widely studied topics in the scientific community due to the settlements, infrastructures and tourist and cultural heritage sites that may be threatened by deformations involving unstable slopes. Engineering geological and geophysical techniques have been recently integrated in multidisciplinary approaches to study gravity-induced slope instability processes and monitor their evolution.

The slope that hosts the Peschiera Springs drainage plant (Central Italy) is involved in a mass rock creep process associated with deep karst dissolution. Due to the importance of this infrastructure, which provides water to the Rome aqueduct, an accelerometric network was installed in 2008, and a nanoseismic array was added in 2014. In this paper, nanoseismic array data were used to determine the location of 397 microseismic events related to the slope instability process, distinguished into two types of events with different

waveforms: 16 failures and 381 collapses. The failures were distributed throughout the slope, while the collapses exhibited two spatially separate clusters below the groundwater level, at a depth where karst processes produce cavities. The clusters were treated as two distinct microseismic sources characterised by specific frequency-magnitude curves of events that describe their attitude to produce events of different magnitudes. Regarding the accelerometric network, an automated procedure was developed for quickly analysing the seismic records, which include signals from teleseisms and near- to far-field earthquakes that can induce deformation in the landslide-involved slope.

The results obtained by the two seismic monitoring systems were integrated with the aim of implementing a landslide hazard matrix based on the statistical frequency of the occurrence of such events and their probability of exceedance during a reference period, providing a useful tool for managing the related landslide risk.

## 1. Introduction

Landslides are a type of major natural hazard, causing large human and economic losses worldwide (Petley, 2012). Guzzetti et al. (2005) studied documents and reports regarding landslides that occurred in Italy between 1279 and 2002 and found that fast-moving landslides in rock slopes (i.e., rockfalls, rockslides, rock avalanches and debris flows) caused the largest number of fatalities, probably due to their quick evolution. Most landslides occur in mountainous areas worldwide (Van Den Eeckhaut et al., 2012), and landslide studies in this environment have been very common because gravity-induced instability processes often threaten strategic infrastructures (Rodríguez-Peces et al., 2011; Bozzano et al., 2012; Delgado et al., 2015).

In recent decades, engineering geological and geophysical techniques have been coupled to study gravity-induced slope instability processes (Bogoslovsky and Ogilvy, 1977; McCann and Forster, 1990; Hack, 2000; Maurer et al., 2010; Jaboyedoff et al., 2019). Contrary to other geophysical techniques that are able to provide 2D or 3D imaging of landslide masses and determine their features (e.g., dimension, geometry, water content or seismic wave velocity), passive seismic techniques can be applied with the aim of detecting variations in specific effects or parameters over time, making them suitable for investigating landslides and for monitoring landslide evolution (Mainsant et al., 2012; Panzera et al., 2012; Burjánek et al., 2018).

In fact, continuous seismic measurements in areas involved in landslide processes can detect the events similar to very weak earthquakes, known as microseismic events, related to the progressive failure and detachment of unstable masses (Senfaute et al., 2009; Amitrano et al., 2010; Got et al., 2010; Lévy et al., 2011). The presence of "marks" in seismic records due to events of a different nature than earthquakes is a well-known issue in seismology. Although national and regional seismic networks are targeted for recording earthquakes, they also allowed to observe seismograms of landslides involving different types of slopes, for example, see Suriñach et al. (2005), Dammeier et al. (2011), Lacroix and Helmstetter (2011), Hibert et al. (2015) or Zhang et al. (2020).

All the above-mentioned studies focus on intense vibrational events, but in the last two decades, the development of specific seismic sensors with high sensitivity has allowed to record microseismic events with low to very low intensity. The widespread deployment of these sensors and their employment in specific networks aimed at landslide monitoring evidenced the occurrence of microseismic events before a main event of slope instability. In this regard, space and time occurrence analysis of microseismic events can be considered a useful tool both for studying the landslide hazard and for managing the related risk by monitoring the failure propagation and the possible occurrence of more critical conditions (i.e., generalised collapse).

The study of microseismicity in rock masses has been performed during mining engineering since the end of the last century and has become widely used in the last two decades (Tezuka and Niitsuma, 2000; Driad-Lebeau et al., 2005; Xu et al., 2015; Zhao et al., 2018). The application of microseismic approaches for monitoring natural gravity-driven instabilities can be more difficult than their application in environments where instability processes are controlled by human activities. As a matter of fact, the induced microseismicity related to human activities (e.g., mining processes, rock excavation, rock hydraulic fracturing) is mainly focused in specific zones of the rock mass where the engineering interventions can induce changes in the stress field, a subsequent opening of new fractures and/or propagation of pre-existing joints and a progressive failure. On the other hand, since such a well-defined trigger (i.e., with a known occurrence in time and space) does not act in rock masses involved in natural landslide processes, the application of microseismic studies to landslide monitoring requires a different approach for investigating and characterising unstable areas.

Since the detection, classification and location of microseismic events is a complex task (Provost et al., 2018), several landslide-involved sites have been instrumented (Spillmann et al., 2007; Helmstetter and Garambois, 2010; Zimmer and Sitar, 2015; Arosio et al., 2018; Colombero, 2018), and experiments have been carried out (Bottelin et al., 2014; Hakes et al., 2018; Guinau et al., 2019) to improve the knowledge in this field. In general, landslide-produced microseismic events are high-frequency signals that cannot be recorded from far distances due to their low energy and fast attenuation; therefore, sensors have to be deployed close enough to the source and have to be analysed with specific tools, software and codes.

In this paper, the results obtained by the monitoring of microseismic events in the landslide-involved slope that hosts the Peschiera Springs drainage plant are presented. The data provided by two independent seismic systems (i.e., a traditional accelerometric network and a nanoseismic monitoring array) were analysed with the aims of i) monitoring the landslide process, ii) assessing the landslide hazard (in terms of probability of occurrence), and iii) managing the related risk.

## 2. Geological and geomorphological setting

The Peschiera Springs are located in the Central Apennines (Italy), approximately 70 km northeast of Rome, on the southwestern flank of Mt. Nuria, in a slope composed of Upper Jurassic and Lower Cretaceous limestones (Bigi and Costa Pisani, 2002) with east-west-trending and north-dipping (30°-40°) strata and faults and thrusts with roughly north-south and northeast-southwest trends (Fig. 1). All the structural elements formed due to past tectonic activities and cannot be classified as active (Bigi and Costa Pisani, 2003), even if minor movements related to moderate/strong regional earthquakes, to teleseisms or to gravity-driven processes may occur. The Nuria-Velino-Fucino-Marsica system discharges a water flow between 18 and 21 $m^3/s$ (Boni et al., 1995) from the Peschiera Springs; a considerable part of this flow is collected by a drainage plant located inside the slope, managed by ACEA S.p.A., for supplying water to the Rome aqueduct.

Field and remote surveys allowed the identification of numerous landforms related to slow, intense and pervasive deformation processes affecting the slope (Lenti et al., 2012). The landform distribution and the measurements performed by a stress-strain monitoring system installed within the drainage plant (Martino et al., 2004; Maffei et al., 2005) were useful to define three specific sectors of the slope at different deformation

stages: i) the southern sector characterised by incipient and low deformations (incipient stage); ii) the western sector with deformations focused at the main trenches or scarps (advanced stage); iii) the eastern sector with very advanced deformation evidenced by scarps, trenches and sinkholes (ultimate stage).

Such a geological evolutionary model testifies that the Peschiera Springs slope is affected by a complex deep-seated gravitational deformation led by a mass rock creep (MRC) process (Chigira, 1992), which began as sackung (Zischinsky, 1969; Savage and Varnes, 1987) and evolved to rock block mass deformation (Martino et al., 2004). The MRC process is associated with the formation of underground caves related to karst dissolution (Maffei et al., 2005; Casini et al., 2006). The ongoing deformation in the advanced MRC slope portion was confirmed by the results obtained by the stress-strain monitoring system (Lenti et al., 2015).

## 3. Seismic monitoring systems

Two independent and permanent seismic networks (Fig. 1) were installed for monitoring the landslide process involving the Peschiera Springs slope: i) a standard accelerometric network and ii) a Seismic Navigating System (SNS) array based on the nanoseismic monitoring technique. Although both systems are able to detect external and internal vibrational events, they are designed to focus their detection capability on different types of events: the accelerometric network is devoted to analysing the most energetic microseismic events originating within the slope and all the events originating outside the slope (i.e., earthquakes) that can induce non-negligible deformations in the MRC-involved rock mass; on the other hand, the SNS array is devoted to detecting all the internal microseismic events (i.e., originating within the slope) that can be related to the MRC evolution itself.

### *3.1. Accelerometric network and alarm system*

On September 2008, an underground accelerometric network was installed in the tunnels of the Peschiera Springs drainage plant. This network is composed of four underground stations (GA, C1, F1 and C6 in Fig. 1) equipped with a 3-component Kinemetrics EpiSensor accelerometer (Fig. 2), with a sensitivity of 2.5 V/g and flat response between 0.1 and 100 Hz, connected to a Kinemetrics Granite digital datalogger set to acquire data at 250 Hz in trigger mode.

As described by Lenti et al. (2012), a Unix script was implemented to distinguish earthquakes and slope-originated microseismic events based on the peak ground acceleration (PGA) values at the different stations, and subsequently, the latter events are divided into failures and collapses based on duration. Then, the events recorded at each station are analysed to compute a daily control index ($CI_{(P,t)}$) based on the number of recorded earthquakes ($FI\_er_{(P,t)}$), number of recorded microseismic events ($FI\_me_{(P,t)}$) and cumulative Arias intensity (AI) of the recorded microseismic events ($EI_{(P,t)}$); finally, a level of alarm is assigned daily at each sector of the drainage plant associated with each station based on the obtained control index ($CI_{(P,t)}$): i) "ordinary" if $CI_{(P,t)}=1$; ii) "alert" if $CI_{(P,t)}=2$; iii) "emergency" if $CI_{(P,t)}=3$. The "emergency" level is reached if the microseismic events have a PGA of $10^{-3}$ g because events with that value have produced visible damage in the drainage plant in the past.

According to Fiorucci et al. (2016b), the accelerometric network recorded 2311 events until September 2015: 1031 earthquakes and 1280 microseismic events related to the MRC process (i.e., failures and collapses). A significant number of collapses was observed during the maximum discharge periods of the Peschiera Springs (i.e., September 2011, June-July 2014 and June-July 2015), testifying to a strict correlation between the collapse occurrence and the water discharge and, consequently, a change in the stress field of the karstified slope due to the groundwater variations. In addition, $CI_{(P,t)}$ often reaches the "emergency" level during these periods, especially in sectors C1 and C6 (Fiorucci et al., 2016b).

On November 2013, three additional 3-component EpiSensor accelerometers (sensitivity 1.25 V/g, flat response between 0.1 and 100 Hz) were installed on the slope surface (stations VGA, VC1 and VC6 in Fig. 1) and integrated into the pre-existing accelerometric network. Such surface stations were not integrated into the control index computation because they showed evident effects of site amplification; therefore, a correction procedure for these stations was proposed and tested in this work (Appendix A). The accelerometric network has been switched off since November 2015 for a main renewal of the drainage plant.

*3.2. Nanoseismic monitoring array*

During 2013, the nanoseismic monitoring technique (Joswig, 2008) was used to study the Peschiera Springs slope by deploying a 27-m-aperture SNS array in the abandoned tunnels of the drainage plant (Fiorucci et al.,

2017). After a training period, a permanent SNS array was installed in 2014 to replace the temporary array (Fig. 1); this permanent array is equipped with 6 single-component Brüel & Kjær 8340 microaccelerometer sensors (Fig. 2), with a high sensitivity (10 V/g) and flat response in a broad frequency range (0.1-1500.0 Hz), connected to a 3-module HBM QuantumX datalogger set to continuously acquire data with a sampling frequency of 600 Hz.

The SNS array records were analysed according to the nanoseismic monitoring approach (Joswig, 2008), a technique developed by the Institute for Geophysics of University of Stuttgart for identifying potential nuclear explosions in the framework of the Comprehensive Test Ban Treaty Organization (CTBTO) activities. Nanoseismic monitoring allows the detection and characterisation of events with extremely low energy, down to an equivalent magnitude $M_L$ of -3.0, also in unfavourable signal-to-noise ratio (SNR) conditions and by using a specific-geometry array called SNS (Joswig, 2008), composed of four stations: a three-component station at the centre of the array surrounded by three outer vertical-component stations, at 120° and with distances ranging from 25 to 100 m from the central station.

The SNS data were managed by NanoseismicSuite software (www.nanoseismic.net), which is composed of two tools: SonoView and HypoLine. SonoView is designed to perform manual event detection by sonogram computation and supersonogram compilation (Sick et al. 2014). A sonogram is a modified spectrogram obtained by several computation steps at each SNS station that removes stationary background noise and allows the identification of events using the "memory image" concept. Then, the four vertical-component sonograms are combined pixel by pixel into a supersonogram that aids in event detection by evidencing the coherence of an event from the base noise. The detected events are localised by HypoLine (Joswig, 2008): fixed a subsoil model, HypoLine indicates the best epicentre solution by drawing 4 circles, 6 hyperboles and 2 beams by picking arrival time and phase of the seismic waves at the 4 stations. Finally, a local magnitude ($M_L$) value is estimated for the analysed event based on the obtained hypocentre using a specific amplitude-distance relation curve produced for near and low-intensity events (Wust-Bloch and Joswig, 2006).

Starting from the original purpose of nuclear explosion detection, in the last ten years, nanoseismic monitoring was tested to characterise microseismic events related to gravity-induced instability processes involving rock cliffs (Wust-Bloch and Joswig, 2006; Wust-Bloch, 2010; Fiorucci et al., 2016a; Hakes et al., 2018; Iannucci et al., 2020) and soil slopes (Walter et al., 2012a, 2012b; Tonnellier, et al. 2013).

After processing with NanoseismicSuite, the microseismic events recorded by the SNS array were also analysed by a specific script using the Seismic Analysis Code (SAC, Goldstein et al., 2003) to obtain their PGA and AI values. Both parameters were computed for each event in the three time histories recorded at the SNS central station; the vertical values ($PGA_v$ and $AI_v$) were computed with the vertical component of the motion, while the horizontal values ($PGA_h$ and $AI_h$) were obtained with the arithmetic mean of the values obtained on the north-south and east-west components.

## 4. Results of the nanoseismic monitoring array

The Peschiera Springs slope represents the only site where a nanoseismic SNS array is installed in a permanent configuration for monitoring a landslide involving a rock slope. Fiorucci et al. (2017) presented the results obtained by the former temporary SNS array as well as the first outputs obtained by the analysis carried out only on the most energic events recorded by the permanent one; however, in this work, the analysis of the permanent SNS array data was extended to all the detected events, regardless of their energy, to obtain a characterisation not only focused on the main microseismic events but also to provide a more exhaustive scenario of the local microseismicity at the Peschiera Springs slope.

### *4.1. Detection and location of microseismic events*

The SNS array at the Peschiera Springs slope detected two typologies of microseismic events originating within the slope and related to gravity-induced instability (Fig. 3), as already distinguished by Lenti et al. (2012) and Fiorucci et al. (2017): i) failures related to rock mass fracturing, with a duration from one to a few seconds, the first part of the signal has a broad frequency content and the coda focuses on low frequencies; ii) collapses, with a duration less than 1 s and a typical waveform of impact with a broad frequency content.

The screening of the SNS seismic data by SonoView allowed the detection of more than 700 microseismic events in 2015, among which only 16 were classified as failures, while most of the microseismic events presented the typical waveform of collapse. Collapses were typically concentrated in specific periods (Fig. 4), causing collapse crises (i.e., occurrence of at least 3 events within 24 h). As reported in Fiorucci et al. (2017), 14 collapse crises were recorded in 2015, mainly between May and July 2015 and in October 2015.

In this paper, the analysis was carried out on 397 events, among which all 16 detected failures and 381 collapses related to different crises occurred between February and July 2015, the period with the maximum number of collapses.

Failures are characterised by a duration of 3-7 s, and their supersonograms output a frequency content between 5 and 200 Hz in the first part of the signal and a coda focused in a lower frequency range, typically between 2 and 50 Hz (Fig. 3). The computed $M_L$ values range from -2.3 to -1.1. The physical analysis of the recorded failures shows that $PGA_h$ and $PGA_v$ range from $10^{-5}$ to $10^{-3}$ m/s$^2$, while $AI_h$ and $AI_v$ vary between $10^{-10}$ and $10^{-8}$ m/s.

On the other hand, the collapse supersonograms indicate that such events are typified by a sudden rise in energy in the whole frequency band of the supersonogram (Fig. 3), between 2 and 225 Hz, according to their paroxysmal and impulsive nature. The collapse length is usually less than 1 s but increases to 3-4 s for multiple or high-intensity events. The $M_L$ values of these events range between -2.8 and -0.3. Considering the physical parameters obtained for collapses, $PGA_h$ and $PGA_v$ are between $10^{-5}$ and $10^{-2}$ m/s$^2$, and $AI_h$ and $AI_v$ are between $10^{-11}$ and $10^{-7}$ m/s.

A simplified model of a homogeneous half-space with a P-wave velocity of 2.6 km/s and S-wave velocity of 1.5 km/s was used to obtain the epicentre and hypocentre coordinates for each microseismic event in HypoLine; such a velocity model was defined based on geophysical investigations commissioned by the drainage plant manager (ACEA S.p.A.) and was tested and validated by Fiorucci et al. (2017).

*4.2. Clustering of microseismic events*

A study on the spatial distribution of the analysed events was carried out to define clusters of microseismic events within the Peschiera Springs slope. Assuming that all the microseismic events of a single cluster originate from the same rock mass volume within the slope and that they are therefore related to a specific deformation process occurring at that location, each cluster can be treated as microseismic sources and characterised in terms of event $M_L$ and frequency. Hudyma and Potvin (2010) proposed a process of spatial clustering in deep mines of Australia and Canada for studying microseismic events induced by mining activities and their related microseismic sources.

In this work, the coordinates of the origin of each event were compared to those of all the other events, and the proximal events were assigned to the same cluster. Such a spatial clustering analysis allowed the exclusion of single and isolated events originating in other portions of the rock mass.

The origin coordinates were obtained for 16 failures and 381 collapses; the two event typologies were treated separately for the spatial clustering analysis because of their different genetic mechanisms in the karst rock mass. The failure events were not clustered due to their low number and dispersion; on the other hand, the collapse clustering analysis allowed us to define two clusters.

Fig. 5 shows the epicentre distribution of the analysed microseismic events at the Peschiera Springs slope; Fig. 6 reports the hypocentres of the analysed microseismic events projected on two geological cross-sections with the groundwater level, which had an average altitude of approximately 420 m a.s.l. during the analysed period. The key elements of the cross-sections were defined by the interpretation of several sources such as scientific publications and reports, engineering geological surveys on the slope surface and inside the tunnels, stress-strain modelling (Martino et al. 2004; Naffrechi et al. 2005) and LiDAR (light detection and ranging) remote surveys (Lenti et al. 2012). The hypocentral uncertainty for microseismic events localised by the SNS array is approximately 10% of the epicentral distance (Walter et al., 2012b); therefore, it ranges between 5 and 25 m for collapses and can also exceed 40 m for farther failures.

Failures are mainly concentrated close to faults and landforms expressed as trenches and subvertical scarps (Fig. 5). Their hypocentres were obtained between 460 and 290 m a.s.l.; in particular, 3 events occurred above the groundwater level, and 13 events originated below the groundwater level (Fig. 6).

Collapses formed 2 different clusters (S1 and S2) in the slope (Fig. 5). Cluster S1 includes 278 collapses and is located in a southern part of the slope characterised by few landforms, where the MRC can be considered to reflect an incipient stage. Cluster S2 incudes 102 collapses and is located in a southwestern zone characterised by an MRC that can be considered to reflect an advanced stage, according to the available measurements recorded along monitored joints indicating an average strain rate of 1 mm/y (Lenti et al., 2015). All the collapse hypocentres were below the groundwater level, at depths between 420 and 360 m a.s.l. (Fig. 6).

The hypocentre variation indicated that collapses occurred in a concentrated layer below the groundwater level, while failures seem not to be directly related to the karst aquifer in the slope. In addition, the

hypocentres of the analysed collapses are localised at a depth where Maffei et al. (2005) evidenced the presence of tensile stresses in the aquifer, which aid karst dissolution and induce the formation of cavities. The obtained results confirm the relation between collapse occurrence and groundwater discharge variations, as already observed by Fiorucci et al. (2017), probably due to the water pressure changes influencing the effective stresses in the karst rock mass.

It was possible to observe separate periods of microseismic activity between the two identified clusters considering the temporal occurrence of the analysed events: the collapses of cluster S1 occurred in five different crises between May and June 2015, while those grouped in cluster S2 occurred in two crises in July 2015.

The two clusters were considered different microseismic sources, and the corresponding relationships between the frequency and the $M_L$ of the events were obtained (Fig. 7a) by drawing linear projections based on the Gutenberg and Richter (1954) power law [Eq. 1]:

$$log_{10} n = a - b\,M \quad [1]$$

where $n$ is the number of events with a magnitude of at least $M$ and $a$ and $b$ are constants.

Cluster S1 is characterised by a roll out at $M_L$ -1.0, a magnitude of completeness ($M_c$) of -2.6 and a constant $b$ of 1.5; cluster S2 is characterised by a roll out at $M_L$ -2.0, a $M_c$ of -2.6 and a constant $b$ of 3.1. Based on the obtained results, compared to cluster S2, cluster S1 seems to be more active in time and characterised by a higher occurrence of events with larger $M_L$. The single event with $M_L$ -0.3 can be considered the most intense event that may be produced by cluster S1. Regardless, neither curve seemed to be sufficiently defined in terms of the number of events. In particular, cluster S1 evidences a lack of events with a $M_L$ value between -1.0 and -0.3, making it difficult to shape a highly reliable and stable linear projection of the frequency-magnitude relation; this lack of data could be due to the limited observation period.

## 5. Integration of the nanoseismic monitoring array and accelerometric network

As highlighted by the results reported above, the nanoseismic monitoring technique represents a reliable tool for investigating gravity-induced instability by defining active rock mass volumes that produce microseismic events. The main advantage of nanoseismic monitoring is that it allows the detection and location of very weak events, providing the most complete characterisation of microseismic events produced by a single

source. On the other hand, this event analysis is a very time-consuming procedure because each microseismic event must be manually localised by an operator after a visual screening of continuously recorded seismic data. Such a disadvantage is an important limit for applying nanoseismic monitoring in a context in which an early warning is required, as for managing the landslide risk in strategic infrastructure such as the drainage plant in the Peschiera Springs slope.

In light of this, an automatic procedure for managing the landslide risk that threatens the drainage plant was specifically implemented by integrating the analysis methods developed for the two independent seismic monitoring systems: the nanoseismic SNS array and the accelerometric network, which is composed of 7 sensors, of which 4 are underground (C6, F1, C1 and GA) at approximately 420 m a.s.l. and 3 are on the slope surface (VC6, VC1 and VGA) between 490 and 550 m a.s.l. Unlike the SNS array, the accelerometric network is not able to detect the weakest events and is automated for detecting and characterising microseismic events as well as for computing a control index based on the events recorded by the 4 underground stations only (Lenti et al., 2012).

After the development of a deconvolution operation aimed at reducing the amplification effects on the signals recorded by the surface stations (Appendix A), a new automatic procedure that includes all the accelerometric network stations was developed for quickly evaluating the active volume of the rock mass (Appendix B). Based on event duration and PGA attenuation, this new automatic procedure associates each microseismic event originating within the Peschiera Springs slope to a station of the accelerometric network and, subsequently, to a volume of rock mass surrounding it. The division of the slope in different volumes was carried out by considering the middle point between adjacent accelerometric stations and drawing a separation plane (Fig. 6). In this way, it is possible to quickly associate an analysed event to a microseismic source discovered by the nanoseismic array.

## 6. Landslide hazard assessment

According to Varnes and IAEG (1984), a hazard indicates the probability of occurrence within a specific period and within a given area of a potentially damaging phenomenon with a given magnitude. In the case of earthquakes, the probability of occurrence of events is computed by using a probabilistic model based on the

Poisson distribution of their magnitude and their statistical distribution over time (Cornell, 1968; Bullen and Bolt, 1985). The following equation [Eq. 2]

$$P_{n\geq 1} = 1 - e^{-\lambda V_R} \quad [2]$$

represents the possibility of occurrence during a reference period $V_R$ of at least one event ($n \geq 1$) having a given magnitude and a frequency $\lambda$ [Eq. 3] of

$$\lambda = \frac{1}{T_R} \quad [3]$$

where $T_R$ is the statistical return period of an event of a specific magnitude.

In this study, a similar approach was applied for evaluating the hazard of the two microseismic sources identified within the Peschiera Springs slope. A function with $V_R$ equal to 1 year was considered based on the observation period; then, a value of $P_{n\geq 1}$ equal to 4% was achieved by fixing a $T_R$value of 25 years. The frequency-$M_L$ curves obtained by the SNS array for S1 and S2 (Fig. 7a) are shaped by cumulating the number of events having at least a given $M_L$; therefore, they can be considered in terms of the probability of exceedance by normalising the event number at each $M_L$ value with respect to all the events generated by each microseismic source during the observation period (Fig. 7b). Source S1 was characterised by an $M_L$ equal to -1.7 and source S2 was characterised by an $M_L$ equal to -2.2 considering a $P_{n\geq 1}$ value of 4%.

Fig. 8 shows the matrix implemented to express the landslide hazard at the drainage plant of the Peschiera Springs slope based on the probabilistic approach adopted to map the earthquake hazard (Montaldo et al., 2007). The x-axis represents the rock mass volumes associated with the accelerometric network stations (Fig. 6). The y-axis represents the microseismic sources defined by the SNS array and is divided based on the MRC evolutionary stage according to Maffei et al. (2005): S1 is located in the volume related to station C1 where the MRC process is in the advanced stage, S2 is located in the volumes of stations C6 and C1 where the MRC process is in the incipient stage. Based on the MRC evolutionary model and past instability events, several hypothetical sources were defined to take into account any possible sources located in the slope: S3 and S4 in the volumes of stations C6-VC6 and C1-VC1-F1, respectively, where the MRC is in the advanced stage; S5 in the volumes of stations GA-VGA where the MRC is in the ultimate stage. A colour scale indicating the different values of intensity of the expected event at a $P_{n\geq 1}$ value of 4% in 1 year is applied. The expected $M_L$ values were obtained from the normalised frequency-$M_L$ curves (Fig. 7), and the minimum

value of $M_L$ was considered the hypothetical source for representing the portions of the slope where no microseismic sources were found.

The proposed matrix allows us to associate a hazard to the microseismic source located in the rock mass volume associated with each microseismic event analysed with the automatic procedure (Appendix B).

The accelerometric network and the SNS array have been switched off since November 2015 and October 2016, respectively, for significant refurbishment work that involves the whole drainage plant; therefore, the produced hazard matrix was tested on a set of events related to the period in which they were working together. The hazard matrix could be modified with the data recorded after the seismic network re-starts, in particular to improve the frequency-$M_L$ curves for the discovered microseismic sources and to confirm and characterise the hypothetical ones.

In light of the presented outputs, the application of the two seismic monitoring systems for managing the landslide risk at the drainage plant of the Peschiera Springs slope is summarised in Fig. 9. The SNS array allows the detection of a large number of microseismic events originating within the slope produced by the MRC evolution, whose analysis allows the evaluation of the landslide hazard. On the other hand, the accelerometric network is able to detect both internal events, even if less accurately than the SNS array, and external events (i.e., earthquakes), whose analysis provides the basis for the alarm system; in this way, the provided alarm system considers the landslide hazard of the slope, related to the MRC evolution and evaluated by the SNS array, as well as the seismic hazard, which can play a role in the slope stability by inducing additional deformations with respect to the MRC.



## 7. Conclusions

In this study, an integrated seismic monitoring system composed of a traditional accelerometric network and a nanoseismic SNS array was used at the drainage plant of the Peschiera Springs slope (Central Apennines, Italy) for recording both earthquakes and internal microseismic events, the former interfering with the large MRC deformation affecting the slope and the latter interfering with the MRC deformation itself.

The SNS array allowed the location of 397 events related to the slope instability, categorized into two different types having different waveforms: 16 failures and 381 collapses. While the failures were distributed across the whole slope, the collapses focused on two different spatial clusters below the groundwater level, at

a depth in which karst processes produce cavities. The clusters were treated as two distinct microseismic sources, and a frequency-magnitude curve of the events was produced for each source. Such curves allowed the definition of the attitude to produce events with different values of magnitude and to assess the magnitude of the maximum expected event, therefore providing information about the different hazards of the two clusters. An automatic procedure was then developed to quickly analyse the events recorded by the accelerometric network and associate them with the microseismic sources identified by the nanoseismic array.

Finally, a landslide hazard matrix was proposed for managing the related risk to the drainage plant in the slope. Such a matrix was implemented considering the different rock mass volumes and microseismic sources with their attitudes to produce events of a given magnitude at a fixed probability of exceedance.

In the framework of landslide risk management, this automatic procedure and hazard matrix may be useful tools for the management of drainage plants (ACEA S.p.A.) to define specific intervention strategies devoted to both increasing the structural resilience of the infrastructure and assuming that intervention protocols are commensurate with the hazard distribution, i.e., based on the active rock mass volumes of interest defined by microseismic events and their spatial distribution, to maintain operation of the drainage plant at the Peschiera Springs slope.

**Acknowledgements**

The authors are grateful to Ing. Giorgio Martino and Dr. Geol. Carlo Romagnoli of ACEA S.p.A. for allowing to perform the here presented analysis and for the provided technical support. The authors wish to thank Institute for Geophysics of University of Stuttgart and Prof. Manfred Joswig for the use of the NanoseismicSuite software. Finally, the authors wish to thank the three anonymous reviewers whose useful and constructive suggestions made possible to improve the original manuscript.

The research was carried on in the framework of: i) the Convention between CERI and ACEA-ATO2 S.p.A. to study the landslide processes affecting the Peschiera Springs slope; ii) the Memorandum of Understanding between CERI and IFSTTAR.

**Author contributions**

This study is part of the Ph.D. research of R. Iannucci funded by the Italian Ministry for Research on the topic “Prevention and forecasting of hydrogeological catastrophes through innovative satellite surveying and web communication systems”.

All the authors contributed to the analytical model conceptualization and to the result interpretation; R. Iannucci and S. Martino defined the engineering geological model and managed the seismic data recording; R. Iannucci and L. Lenti designed the seismic data analysis; R. Iannucci performed the seismic data processing.

**References**

Amitrano, D., Arattano, M., Chiarle, M., Mortara, G., Occhiena, C., Pirulli, M., Scavia, C., 2010. Microseismic activity analysis for the study of the rupture mechanism in unstable rock masses. Nat. Hazard Earth Syst. Sci., 10, 831-841

Arosio, D., Longoni, L., Papini, M., Boccolari, M., Zanzi, L., 2018. Analysis of microseismic signals collected on an unstable rock face in the Italian Prealps. Geophys. J. Int., 213(1), 475-488

Bigi, S., Costa Pisani, P., 2002. Structural setting of the Cicolano-M. Calvo area (Central Apennines, Italy). Boll. Soc. Geol. It., Spec. 1, 141-149

Bigi, S., Costa Pisani, P., 2003. The «pre-thrusting» Fiamignano normal fault. Boll. Soc. Geol. It., 122(2), 267-276

Bogoslovsky, V.A., Ogilvy, A.A., 1977. Geophysical methods for the investigation of landslides. Geophysics, 42(3), 562–571

Boni, C.F., Capelli, G., Petitta, M., 1995. Carta idrogeologica dell’alta e media Valle del F. Velino. System. Cart., Roma (IT)

Bottelin, P., Jongmans, D., Daudon, D., Mathy, A., Helmstetter, A., Bonilla-Sierra, V., Cadet, H., Amitrano, D., Richefeu, V., Lorier, L., Baillet, L., Villard, P., Donzé, F., 2014. Seismic and mechanical studies of the artificially triggered rockfall at Mount Néron (French Alps, December 2011). Nat. Hazards Earth Syst. Sci., 14(12), 3175-3193

Bozzano, F., Martino, S., Montagna, A., Prestininzi, A., 2012. Back analysis of a rock landslide to infer rheological parameters. Eng. Geol., 131, 45-56

Bullen, K.E., Bolt, B.A., 1985. An introduction to the theory of seismology. Cambridge University Press, Cambridge (UK)

Burjánek, J., Gischig, V., Moore, J.R., Fäh, D., 2018. Ambient vibration characterization and monitoring of a rock slope close to collapse. Geophys. J. Int., 212 (1), 297-310

Casini, S., Martino, S., Petitta, M., Prestininzi, A., 2006. A physical analogue model to analyses interactions between tensile stresses and dissolution in carbonate slopes. Hydrogeol. J., 14, 1387-1402

Chigira, M., 1992. Long term gravitational deformations of rock mass by mass rock creep. Eng. Geol., 32, 157-184

Colombero, C., Comina, C., Vinciguerra, S., Benson, P.M., 2018. Microseismicity of an unstable rock mass: From field monitoring to laboratory testing. J. Geophys. Res., 123(2), 1673-1693

Cornell, C.A., 1968. Engineering seismic risk analysis. Bull. Seism. Soc. Am., 58(5), 1583-1606

Dammeier, F., Moore, J.R., Haslinger, F., Loew, S. 2011. Characterization of alpine rockslides using statistical analysis of seismic signals. J. Geophys. Res., 116(F40), F04024

Delgado, J., Garrido, J., Lenti, L., Lopez-Casado, C., Martino, S., Sierra, F.J., 2015. Unconventional pseudostatic stability analysis of the Diezma landslide (Granada, Spain) based on a high-resolution engineering geological model. Eng. Geol., 194, 81-95

Driad-Lebeau, L., Lahaie, F., Al Heib, M., Josien, J.P., Bigarre, P., Noirel, J.F., 2005. Seismic and geotechnical investigations following a rockburst in a complex French mining district. Int. J. Coal. Geol., 64(1), 66-78

Fiorucci, M., Iannucci, R., Martino, S., Paciello, A., 2016a. Detection of nanoseismic events related to slope instabilities in the quarry district of Coreno Ausonio (Italy). Italian Journal of Engineering Geology and Environment, 2, 51-63

Fiorucci, M., Iannucci, R., Martino, S., Prestininzi, A., Rivellino, S., Lenti, L., Paciello, A., 2016b. Integrated seismic monitoring system in a major aqueduct infrastructure, in Landslides and Engineered Slopes. Experience, Theory and Practice, pp 917-924, eds Aversa, S., Cascini, L., Picarelli, L., Scavia, C., CRC Press/Balkema, Leiden (Netherlands)

Fiorucci, M., Iannucci, R., Lenti, L., Martino, S., Paciello, A., Prestininzi, A., Rivellino, S., 2017. Nanoseismic monitoring of gravity-induced slope instabilities for the risk management of an aqueduct infrastructure in Central Apennines (Italy). Nat. Hazards, 86(S2), 345-362

Goldstein, P., Dodge D, Firpo M, Minner L., 2003. SAC2000: Signal processing and analysis tools for seismologists and engineers, in The IASPEI International Handbook of Earthquake and Engineering Seismology, eds Lee, W.H.K., Kanamori H., Jennings P.C., Kisslinger C., Academic Press, London (UK)

Got, J.-L., Mourot, P., Grangeon, J., 2010. Pre-failure behaviour of an unstable limestone cliff from displacement and seismic data. Nat. Hazards Earth Syst. Sci., 10, 819-829

Guinau, M., Tapia, M., Pérez-Guillén, C., Suriñach, E., Roig, P., Khazaradze, G., Torné, M., Royán, M.J., Echeverria, A., 2019. Remote sensing and seismic data integration for the characterization of a rock slide and an artificially triggered rock fall. Eng. Geol., 257, 105142

Gutenberg, B., Richter, C.F., 1954. Seismicity of the Earth and associated phenomena. Princeton University Press, Princeton (USA)

Guzzetti, F., Stark, C.P., Salvati, P., 2005. Evaluation of Flood and Landslide Risk to the Population of Italy. Environ. Manage, 36(1), 15-36

Hack, R., 2000. Geophysics for slope stability. Surv. Geophys., 21, 423-448

Hakes, C., Fiorucci, M., Iannucci, R., Martino, S., Paciello, A., 2018. Nanoseismic monitoring for detection of rockfalls: experiments in quarry areas. Italian Journal of Engineering Geology and Environment, 1, 39-52

Helmstetter, A., Garambois, S. 2010. Seismic monitoring of Séchilienne rockslide (French Alps): Analysis of seismic signals and their correlation with rainfalls. J. Geophys. Res., 115(F3), F03016

Hibert, C., Stark, C.P., Ekström, G., 2015. Dynamics of the Oso-Steelhead landslide from broadband seismic analysis. Nat. Hazards Earth Syst. Sci., 15(6), 1265-1273

Hudyma, M., Potvin, Y.H., 2010. An engineering approach to seismic risk management in hardrock mines. Rock Mech. Rock Eng., 43, 891-906

Iannucci, R., Martino, S., Paciello, A., D'Amico, S., Galea, P., 2020. Investigation of cliff instability at Għajn Ħadid Tower (Selmun Promontory, Malta) by integrated passive seismic techniques. J. Seismol., DOI: 10.1007/s10950-019-09898-z

Jaboyedoff, M., Del Gaudio, V., Derron, M. H., Grandjean, G., Jongmans, D., 2019. Characterizing and monitoring landslide processes using remote sensing and geophysics. Eng. Geol., 259, 105167

Joswig, M., 2008. Nanoseismic monitoring fills the gap between microseismic networks and passive seismic. First Break, 26, 121-128

Lacroix, P., Helmstetter, A., 2011. Location of seismic signals associated with microearthquakes and rockfalls on the Séchilienne landslide, French Alps. Bull. Seism. Soc. Am., 101(1), 341-353

Lenti, L., Martino, S., Paciello, A., Prestininzi, A., Rivellino, S., 2012. Microseismicity within a karstified rock mass due to cracks and collapses triggered by earthquakes and gravitational deformations. Nat. Hazards, 64, 359-379

Lenti, L., Martino, S., Paciello, A., Prestininzi, A., Rivellino, S., 2015. Recorded displacements in a landslide slope due to regional and teleseismic earthquakes. Geophys. J. Int., 201, 1335-1345

Lévy, C., Jongmans, D., Baillet, L., 2011. Analysis of seismic signals recorded on a prone-to-fall rock column (Vercors massif, French Alps). Geophys. J. Int., 186, 296-310

Maffei, A., Martino, S., Prestininzi, A., 2005. From the geological to the numerical model in the analysis of the gravity-induced slope deformations: an example from the Central Apennines (Italy). Eng., Geol., 78, 215-236

Mainsant, G., Larose, E., Brönnimann, C., Jongmans, D., Michoud, C., Jaboyedoff, M., 2012. Ambient seismic noise monitoring of a clay landslide: Toward failure prediction. J. Geophys. Res., 117(F1), F01030

Martino, S., Prestininzi, A., Scarascia Mugnozza, G., 2004. Geological-evolutionary model of a gravity-induced slope deformation in the carbonate central Apennines (Italy). Q. J. Eng. Geol. Hydrogeol., 37(1), 31-47

Maurer, H., Spillmann, T., Heincke, B., Hauck, C., Loew, S., Springman, S.M., Green, A.G., 2010. Geophysical characterization of slope instabilities. First Break, 28(8), 53-61

McCann, D.M., Forster, A., 1990. Reconnaissance geophysical methods in landslide investigations. Eng. Geol., 29, 59-78

Montaldo, V., Meletti, C., Martinelli, F., Stucchi, M., Locati, M., 2007. On-line seismic hazard data for the new Italian building code. J. Earthq. Eng., 11(S1), 119-132

Panzera, F., D'Amico, S., Lotteri, A., Galea, P., Lombardo, G., 2012. Seismic site response of unstable steep slope using noise measurements: the case study of Xemxija Bay area, Malta. Nat. Hazards Earth Syst. Sci., 12, 3421–3431

Petley, D., 2012. Global patterns of loss of life from landslides. Geology, 40, 927-930

Provost, F., Malet, J.P., Hibert, C., et al., 2018. Towards a standard typology of endogenous landslide seismic sources. Earth Surf. Dyn., 6, 1059-1088

Rodríguez-Peces, M.J., Azañón, J.M., García-Mayordomo, J., Yesares, J., Troncoso, E., Tsige, M., 2011. The Diezma landslide (A-92 motorway, Southern Spain): history and potential for future reactivation. Bull. Eng. Geol. Environ., 70, 681-689

Savage, W.Z., Varnes, D.J., 1987. Mechanism of gravitational spreading of steep-sided ridges ("sackung"). Bull. Int. As. Eng. Geol., 35, 31-36

Senfaute, G., Duperret, A., Lawrence, J.A., 2009. Micro-seismic precursory cracks prior to rock-fall on coastal chalk cliffs: a case study at Mesnil-Val, Normandie, NW France. Nat. Hazards Earth Syst. Sci., 9, 1625-1641

Sick, B., Walter, M., Joswig, M., 2014. Visual event screening of continuous seismic data by supersonograms. Pure Appl. Geophys., 171, 549-559

Spillmann, T., Maurer, H., Green, A.G., Heincke, B., Willenberg, H., Husen, S., 2007. Microseismic investigation of an unstable mountain slope in the Swiss Alps. J. Geophys. Res., 112(B7), B07301

Suriñach, E., Vilajosana, I., Khazaradze, G., Biescas, B., Furdada, G., Vilaplana, J.M., 2005. Seismic detection and characterization of landslides and other mass movements. Nat. Hazards Earth Syst. Sci., 5(6), 791-798

Tezuka, K., Niitsuma, H., 2000. Stress estimated using microseismic clusters and its relationship to the fracture system of the Hijiori hot dry rock reservoir. Eng. Geol., 56 (1-2), 47-62

Tonnellier, A., Helmstetter, A., Malet, J.-P., Schmittbuhl, J., Corsini, A., Joswig, M., 2013. Seismic monitoring of soft-rock landslides: the Super-Sauze and Valoria case studies. Geophys. J. Int., 193(3), 1515-1536

Van Den Eeckhaut, M., Hervas, J., Jaedicke, C., Malet, J.-P., Montanarella, L., Nadim, F., 2012. Statistical modelling of Europe-wide landslide susceptibility using limited landslide inventory data. Landslides, 9, 357-369

Varnes, D.J., IAEG, 1984. Landslide hazard zonation: a review of principles and practice. United Nations Scientific and Cultural Organization, Quetigny (FR)

Walter, M., Schwaderer, U., Joswig, M., 2012a. Seismic monitoring of precursory fracture signals from a destructive rockfall in the Vorarlberg Alps, Austria. Nat. Hazards Earth Syst. Sci., 12, 3545-3555

Walter, M., Arnhardt, C., Joswig, M., 2012b. Seismic monitoring of rockfalls, slide quakes and fissure development at the Super-Sauze mudslide, French Alps. Eng. Geol., 128, 12-22

Wust-Bloch, G.H., 2010. Characterizing and locating very weak ($-2.2 \geq M_L \geq -3.4$) induced seismicity in unstable sandstone cliffs by nanoseismic monitoring. Pure Appl. Geophys., 167, 153-167

Wust-Bloch, G.H., Joswig, M., 2006. Pre-collapse identification of sinkholes in unconsolidated media at Dead Sea area by 'nanoseismic monitoring' (graphical jackknife location of weak sources by few, low-SNR records). Geophys. J. Int., 167, 1220-1232

Xu, N.W., Li, T.B., Dai, F., Li, B., Zhu, Y.G., Yang, D.S., 2015. Microseismic monitoring and stability evaluation for the large scale underground caverns at the Houziyan hydropower station in Southwest China. Eng. Geol., 188, 48-67

Zhang, Z., He, S., Li, Q., 2020. Analyzing high-frequency seismic signals generated during a landslide using source discrepancies between two landslides. Eng. Geol., 272, 105640.

Zhao, J.S., Feng, X.T., Jiang, Q., Zhou, Y.Y., 2018. Microseismicity monitoring and failure mechanism analysis of rock masses with weak interlayer zone in underground intersecting chambers: A case study from the Baihetan Hydropower Station, China. Eng. Geol., 245, 44-60

Zimmer, V.L., Sitar, N., 2015. Detection and location of rock falls using seismic and infrasound sensors. Eng. Geol., 193, 49-60

Zischinsky, U., 1969. Uber Sackungen. Rock Mech., 1, 30-52

**Appendix A. Procedure for correcting site amplification effects for the signals recorded by the accelerometric network stations**

The use of the surface accelerometric station (VC6, VC1 and VGA) required a preliminary correction for removing any possible amplification effects due to topographic features and to the installation on the jointed rock mass. This correction was carried out by computing for each station a specific deconvolution function based on a set of 15 earthquakes originating farther than 40 km from the slope (Tab. 1), since the attenuation inside the slope is negligible with respect to the attenuation between the origin and the slope.

By analysing the PGA values computed with SAC for these far-field earthquakes (Fig. A.1a), it was possible to observe that the stations installed on the slope surface (VC6, VC1 and VGA) show systematically higher PGA values than the underground stations installed inside the drainage plant (C6, F1, C1 and GA), confirming the presence of site amplification effects.

To evaluate the amplification effects, the parameter $E_r$ was defined according to the following equation [Eq. A.1]:

$$E_r = \frac{PGA_{STA} - PGA_{REF}}{PGA_{REF}} \cdot 100 \qquad [A.1]$$

where $PGA_{STA}$ represents the PGA value recorded at the considered station and $PGA_{REF}$ represents the PGA value recorded at the reference station. Such a parameter quantifies the percentage difference in PGA values between a station and a reference station and is computed for homologous components. Station F1 was chosen as the reference station, and $E_r$ was computed for all the far-field earthquakes with homologous spatial components. The term reference station does not have a seismological meaning; here, it indicates a station that does not evidence marked amplification effects and is located in a central position within the slope. Fig. A.2a shows the variation in the $E_r$ parameters between several stations of the network, evidencing a non-negligible PGA amplification for the stations on the slope surface and for station C1Y with respect to the reference.

For the surface stations (VC6, VC1 and VGA), the amplification effects seem to be greater for the horizontal components than for the vertical ones. In fact, the mean $E_r$ value is between 68.65% and 164.15% for the vertical components and between 140.43% and 853.25% for the horizontal components. For the underground stations (C6, F1, C1 and GA), the mean $E_r$ varies between 21.97% and 33.83% for the vertical components

and between 12.72% and 38.37% for the horizontal components, except for C1Y, which shows an average $E_r$ value of 70.03%.

A complex function $R$ was defined according to Eq. A.2 to remove amplification effects:

$$R(\omega) = \frac{STA(\omega)}{REF(\omega)} \quad [A.2]$$

representing the ratio between the Fourier transform of a signal recorded at a given station $STA$ and the same signal recorded at the reference station $REF$.

Considering the specific $R_m$ function for each component of each station, it is possible to report to the reference station any event recorded in the considered station by the following equation [Eq. A.3]:

$$STA_{CONV}(\omega) = \frac{STA(\omega)}{R_m(\omega)} \quad [A.3]$$

in which $STA_{CONV}$ represents the signal reported to the reference station $REF$ by applying, in the frequency domain, the ratio between the original signal recorded at the considered station $STA$ and its own function $R_m$.

The different $R_{eq}$ functions were computed for each far-field earthquake recorded at a given station [Eq. A.4] using SAC:

$$R_{eq}(\omega) = \frac{STA_{eq}(\omega)}{REF_{eq}(\omega)} \quad [A.4]$$

and the resulting Fourier transform was expressed via the amplitude and phase [Eq. A.5]:

$$R_{eq}(\omega) = \frac{A_{eq,STA}(\omega) \cdot e^{i\varphi_{eq,STA}(\omega)}}{A_{eq,REF}(\omega) \cdot e^{i\varphi_{eq,REF}(\omega)}} \quad [A.5]$$

This expression is solvable in the following form [Eq. A.6]:

$$R_{eq}(\omega) = \left(\frac{A_{eq,STA}(\omega)}{A_{eq,REF}(\omega)}\right) \cdot e^{i\left(\varphi_{eq,STA}(\omega) - \varphi_{eq,REF}(\omega)\right)} \quad [A.6]$$

Finally, the mean $R_m$ complex function was computed by averaging the different $R_{eq}$ related to the 15 far-field earthquakes recorded at station $STA$ by the following equation [Eq. A.7]:

$$R_m = \frac{\sum_{i=1}^{15} R_{eq,i}(\omega)}{15} \quad [A.7]$$

Then, the $R_m$ complex functions, obtained for each component of each station, were applied by a deconvolution operation to report the far-field earthquakes to the reference, according to Eq. A.3. The

deconvolution operation was applied only on the signals recorded by the surface stations and for component C1Y, which evidenced site amplification effects.

Comparing the PGA values determined before (Fig. A.1a) and after (Fig. A.1b) deconvolution, it is possible to observe the removal of the amplification effects. In fact, the records of the stations installed on the slope surface after the performed deconvolution show PGA values similar to those of the stations installed inside the drainage plant. In addition, the variation in the $E_r$ parameter [Eq. A.1] seems to be similar for all the stations after the deconvolution (Fig. A.2b), especially if compared with the values computed with the original time histories (Fig. A.2a). For the slope surface stations, the mean $E_r$ value computed after the deconvolution operation is between 115.45% and 130.65% for the vertical components and between 83.07% and 145.65% for the horizontal components, evidencing a marked decrease with respect to the values computed before the deconvolution operation. Even component C1Y shows a decrease in its mean $E_r$ value. These results demonstrate that the deconvolution operation reduces the site amplification effects of the considered signals.

The $R_m$ complex functions computed here are applied in Appendix B for carrying out a deconvolution of the time histories of different types of events (i.e., near-field earthquakes, collapses and failures) recorded by the surface accelerometric stations and by component C1Y to obtain time histories not perturbed by site amplification effects.

**Appendix B. Automatic procedure for analysing events recorded by the accelerometric network**

A procedure for quickly evaluating the source of the events recorded by the accelerometric network was designed after the definition of the amplification effect correction functions for the signals recorded by the surface stations and component C1Y (Appendix A). Such a procedure does determine the hypocentre of the analysed event and only provides the volume of the rock mass from which it originates. The procedure, implemented with the Unix platform through specific scripts for SAC, MATLAB and Fortran codes, is able to distinguish the type of event (i.e., earthquake, collapse, or failure) based on the analysis of the attenuation at the different network stations and on the duration; then, the event is associated with a certain volume of the slope based on the maximum value of the PGA obtained after the deconvolution.

The procedure is illustrated in the flow chart of Fig. B.1. Each block has a code, and its shape indicates a different type of operation:

- rectangle for the start and end of the procedure;
- ellipse for reading and/or writing operations;
- parallelogram for the analysis process;
- rhombus for control and/or choice operations.

The input (L1) is represented by a list of N events recorded by the accelerometric network. The procedure starts a main cycle in which each event is analysed separately. Since each event consists of 21 time histories (3 components for the 7 stations), the procedure analyses one time history at a time. In block A1, the amplification effects are removed by applying the defined $R_m$ complex functions (Appendix A), and three values are computed:

- $PGA_{or}$, representing the PGA value of the original time history;
- $PGA_{head}$, representing the PGA value of the original time history between 2 and 12 s;
- $PGA_{conv}$, representing the PGA value of the convoluted time history.

Based on these PGA values, two control indexes are assigned to the analysed time history. Index $I_{PGA}$ depends on the ratio $R_{PGA}$, defined as [Eq. B.1]:

$$R_{PGA} = \frac{PGA_{or}}{PGA_{head}} \qquad [B.1]$$

Since typical collapses are not recorded by all accelerometric stations, $R_{PGA}$ allows us to define whether an event exists in the time history ($I_{PGA}$=1 when $R_{PGA}$≥1.5) or if the time history contains only seismic ambient noise ($I_{PGA}$=0 when $R_{PGA}$<1.5). In the latter case, the time history is excluded by the subsequent analyses.

Index $I_{ER}$ is assigned based on the parameter $E_r$, which is defined by Eq. A.1. Parameter $E_r$ is computed for the time history after the deconvolution operation and indicates the difference between $PGA_{conv}$ at that considered station and $PGA_{conv}$ at the reference station. Then, this value is compared with those obtained for the far-field earthquakes (Fig. A.2b): $I_{ER}$ is equal to 0 if the obtained $E_r$ value is between the standard deviation range of $E_r$ computed for the far-field earthquakes; otherwise, $I_{ER}$ is equal to 1.

In block C1, a value of index $I_{EV}$ is assigned based on the other two previously introduced indexes:

- $I_{EV}$=0, if $I_{PGA}$=0, the time history contains only seismic ambient noise;
- $I_{EV}$=1, if $I_{PGA}$=1 and $I_{ER}$=0, the time history is statistically in the range of $E_r$ related to earthquakes and may thus correspond to an earthquake;
- $I_{EV}$=2, if $I_{PGA}$=1 and $I_{ER}$=1, the time history is statistically outside the range of $E_r$ related to earthquakes and may thus correspond to an event originating within the slope.

This distinction is possible because events originated within the slope (i.e., collapses and failures) are characterised by a fast attenuation into the slope and therefore produce PGA values significantly different between the 7 accelerometric stations, depending on the proximity of the recorded event. In contrast, earthquakes originate at distances longer than the slope dimensions; therefore, their attenuation in the slope can be considered negligible compared to the attenuation that occurs along the path between the origin and the slope.

The procedure performs the previously described analyses on the 21 time histories of an event and then moves onto block C2 in which all 21 values of the index $I_{EV}$ are considered and the parameter $R_{EV}$ is defined according to the following equation [Eq. B.2]:

$$R_{EV} = \frac{\#2}{\#T} \cdot 100 \qquad [B.2]$$

where $\#2$ represents the number of time histories with an $I_{EV}$ equal to 2 and $\#T$ represents the number of time histories with an $I_{EV}$ equal to 1 or 2. Parameter $R_{EV}$ is used to identify the event based on a statistic determined from all 21 time histories of the event. The event originates within the slope if $R_{EV}$ is equal to or

larger than 60%; therefore, this event is a collapse or a failure. The event is an earthquake if $R_{EV}$ is less than 60%. The threshold value of 60% was tested on a set of 15 far-field earthquakes (epicentre farther than 40 km), 16 near-field earthquakes (epicentre nearer than 40 km), 15 collapses and 16 failures, outputting an incorrect solution only for 3 weak earthquakes with an epicentre less than 5 km from the slope.

If $R_{EV}$ is less than 60%, the procedure moves on to block L3, and the event is defined as an earthquake whose features (e.g., epicentre, hypocentre, and magnitude) can be obtained from the National Institute of Geophysics and Volcanology (INGV) website (http://cnt.rm.ingv.it/).

If $R_{EV}$ is at least 60%, the procedure performs the Hilbert transform in analysis block A3 and then moves on to control block C3 for the evaluation of the event duration: the event is classified as a collapse if the duration is less than 1 s, while the event is classified as a failure if the duration is more than 1 s. In both cases, the procedure passes to analysis block A4 for assessing the station in which the greatest resentment occurred. In that block, the norm of the $PGA_{conv}$ values is computed as [Eq. B.3]:

$$PGA_{conv,NOR} = \sqrt[2]{(PGA_{conv,NS})^2 + (PGA_{conv,EW})^2 + (PGA_{conv,Z})^2} \qquad [B.3]$$

where $PGA_{conv,NOR}$ is the PGA norm at the station and $PGA_{conv,NS}$, $PGA_{conv,EW}$ and $PGA_{conv,Z}$ are the three values of $PGA_{conv}$ computed for the three motion components. The analysed event is assigned to the accelerometric station that presents the maximum $PGA_{conv,NOR}$ value.

At this point, the procedure returns to block L1 and re-starts the whole cycle of analyses for all $N$ events in the input list.

Fig. 1 Geological map of the Peschiera Springs slope: 1) recent alluvial deposits (Holocene); 2) eluvio-colluvial deposits and reddish soils (Holocene); 3) slope debris (upper Pleistocene-Holocene); 4) Fosso Canalicchio Formation (upper Pliocene-lower Pleistocene); 5) sandy-clayey flysch (upper Miocene); 6) marly limestone, marl and calcarenite (lower Miocene); 7) Scaglia Formation (Upper Cretaceous-lower Miocene); 8) Salpingoporella and birdseye limestone (Lower Cretaceous); 9) coral and echinoid limestone (Upper Jurassic); 10) fault; 11) thrust; 12) supposed fault; 13) attitude of strata; 14) MRC limit in advanced stage; 15) underground accelerometric network station; 16) surface accelerometric network station; 17) underground SNS array station; 18) cross-section (see Fig. 6).

Double column

Fig. 2 Seismic monitoring systems: (a) accelerometric network station; (b) temporary and permanent SNS array stations.

Single column

Fig. 3 From top to bottom, supersonogram and sonograms with overlaid time histories of the two event types detected by the nanoseismic array: failure occurred on July 9th, 2015, (left) and collapse occurred on July 3rd, 2015 (right). The upper 3 time histories are recorded by the 3 outer vertical-component stations, and the lower 3 time histories are recorded by the central 3-component station.

Double column

Fig. 4 Supersonogram from 14:30 UTC to 15:08 UTC on July 3rd, 2015, obtained by the SNS array; the blue frames indicate collapses.

Double column

Fig. 5 Satellite view of the Peschiera Springs slope showing 1) recent alluvial deposits; 2) reddish soils; 3) slope debris; 4) trench; 5) tension crack; 6) sinkhole; 7) 1997 sinkhole; 8) scarp; 9) MRC limit in advanced stage; 10) fault (dashed where supposed); 11) underground accelerometric network station (with ID); 12) surface accelerometric network station (with ID); 13) underground SNS array station; 14) failure epicentre;

15) collapse epicentre related to cluster S1; 16) collapse epicentre related to cluster S2; 17) cross-section (see Fig. 6).

Double column

Fig. 6 Geological cross-sections of the Peschiera Springs slope (see Figs. 1 and 5) showing 1) recent alluvial deposits; 2) slope debris, trench debris and reddish soils; 3) intensely jointed rock mass of Salpingoporella and birdseye limestone; 4) rarely jointed rock mass of Salpingoporella and birdseye limestone; 5) rock mass with MRC in advanced stage; 6) rock mass with underground cavities formation; 7) fault (dashed where supposed); 8) groundwater level; 9) underground accelerometric network station; 10) surface accelerometric network station; 11) central station of the SNS array; 12) collapse epicentre related to cluster S1; 13) collapse epicentre related to cluster S2; 14) failure epicentre; 15) rock mass volume separation.

Double column

Fig. 7 Graphics of the number of events having at least a given $M_L$ (a) and normalised number of events having at least a given $M_L$ (b) for cluster S1 (left) and cluster S2 (right); the dashed grey lines indicate the considered $P_{n\geq 1}$ value and the relative $M_L$ value.

Double column

Fig. 8 Landslide hazard matrix proposed for assessing the landslide hazard at the Peschiera Springs slope; the asterisks indicate hypothesised values.

1.5 column

Fig. 9 Flow chart summarising the application of the SNS array and of the accelerometric network for managing the landslide risk at the drainage plant of the Peschiera Springs slope.

1.5 column

Fig. A.1 PGA values of the 15 far-field earthquakes recorded by the accelerometric network of the Peschiera Springs slope computed with the original time histories (a) and on the deconvoluted time histories (b).

Single column

Fig. A.2 Values (grey dots), average value (red dot) and standard deviation (red bar) of $E_r$ computed for the 15 far-field earthquakes recorded by the accelerometric network of the Peschiera Springs slope before (a) and after (b) the deconvolution operation.

Double column

Fig. A.3 Flow chart explaining the procedure of defining the source for the events recorded by the accelerometric network of the Peschiera Springs slope.

1.5 column

| Day | UTC time | Source | Lat | Long | Depth (km) | M | Distance (km) |
|---|---|---|---|---|---|---|---|
| 26/03/2014 | 02:59:17 | Martani | 42.789 | 12.536 | 6.7 | 3 | 60.9 |
| 01/04/2014 | 22:51:10 | Martani | 42.781 | 12.544 | 7.2 | 3.1 | 58.9 |
| 02/04/2014 | 02:10:48 | Martani | 42.789 | 12.527 | 6.7 | 3.1 | 61.3 |
| 15/04/2014 | 08:10:34 | Colfiorito | 42.975 | 12.912 | 9.1 | 3.3 | 68.1 |
| 19/04/2014 | 21:28:00 | Gubbio | 43.349 | 12.534 | 7.9 | 3.7 | 116.2 |
| 14/06/2014 | 08:51:50 | Martani | 42.669 | 12.548 | 7.2 | 3.5 | 50.9 |
| 18/09/2014 | 21:46:35 | Norcia | 42.769 | 13.103 | 9.9 | 2.7 | 46 |
| 24/12/2014 | 11:40:40 | Frentani | 41.707 | 14.956 | 18 | 4 | 177.4 |
| 28/02/2015 | 03:16:01 | Fucino | 41.95 | 13.534 | 10.6 | 4.1 | 63.5 |
| 18/03/2015 | 04:03:40 | Norcia | 42.718 | 13.048 | 9.9 | 2.5 | 40 |
| 07/04/2015 | 07:45:25 | Tivoli | 41.923 | 12.715 | 15.7 | 2.5 | 55.1 |
| 08/04/2015 | 14:30:13 | Sibillini | 42.875 | 13.29 | 7.8 | 3.2 | 61.4 |
| 08/05/2015 | 04:58:25 | Laga | 42.781 | 13.539 | 20.4 | 3 | 63.7 |
| 21/05/2015 | 09:42:11 | A. Piceno | 43.044 | 13.314 | 21.5 | 3.4 | 79.5 |
| 19/09/2015 | 07:22:00 | Urbino | 43.628 | 12.335 | 7.1 | 3.7 | 150.7 |

Tab. A.1 Set of the 15 earthquakes recorded by the accelerometric network with an epicentre farther than 40 km from the Peschiera Springs slope; hypocentre, epicentre and M values were obtained by the INGV website (http://cnt.rm.ingv.it/).

**Declaration of interests**

☒ The authors declare that they have no known competing financial interests or personal relationships that could have appeared to influence the work reported in this paper.

☐The authors declare the following financial interests/personal relationships which may be considered as potential competing interests:

**Author contributions**

This study is part of the Ph.D. research of R. Iannucci funded by the Italian Ministry for Research on the topic “Prevention and forecasting of hydrogeological catastrophes through innovative satellite surveying and web communication systems”.

All the authors contributed to the analytical model conceptualization and to the result interpretation; R. Iannucci and S. Martino defined the engineering geological model and managed the seismic data recording; R. Iannucci and L. Lenti designed the seismic data analysis; R. Iannucci performed the seismic data processing.

**Highlights**

- Analysis of microseismic events recorded by two seismic systems in an unstable slope.

- Assessing of landslide hazard by microseismic event analysis.

- Implementation of an automatic procedure to analyse microseismic events.

- Integration of seismic systems to manage the drainage plant located within the slope.